High-efficiency *In Vitro* and *In Vivo* Detection of Zn^{2+} by Dye-assembled Upconversion Nanoparticles

Juanjuan Peng[§,‡], Wang Xu[†,‡], Chai Lean Teoh[§], Sanyang Han[†], Beomsue Kim[§], Animesh Samanta[§], Jun Cheng Er[†], Lu Wang[†], Lin Yuan[†], Xiaogang Liu[†,#,Φ], and Young-Tae Chang[§,†,*]

§ Singapore Bioimaging Consortium, Agency for Science, Technology and Research (A* STAR), 138667, Singapore.

† Department of Chemistry, National University of Singapore, 117543, Singapore.

Institute of Materials Research and Engineering, Agency for Science, Technology and Research (A* STAR), 117602, Singapore.

Φ Center for Functional Materials, NUS (Suzhou) Research Institute, Suzhou, Jiangsu 215123, China

ABSTRACT: Development of highly sensitive and selective sensing systems of divalent zinc ion (Zn^{2+}) in organisms has been a growing interest in the past decades owing to its pivotal role in cellular metabolism, apoptosis and neurotransmission. Herein, we report the rational design and synthesis of a Zn^{2+} fluorescent-based probe by assembling lanthanide-doped upconversion nanoparticles (UCNPs) with chromophores. Specifically, upconversion luminescence (UCL) can be effectively quenched by the chromophores on the surface of nanoparticles *via* a fluorescence resonant energy transfer (FRET) process and subsequently recovered upon the addition of Zn^{2+}, thus allowing for quantitative monitoring of Zn^{2+}. Importantly, the sensing system enables detection of Zn^{2+} in real biological samples. We demonstrate that this chromophore-UCNP nanosystem is capable of implementing an efficient *in vitro* and *in vivo* detection of Zn^{2+} in mouse brain slice with Alzheimer's disease and zebrafish, respectively.

■ INTRODUCTION

As the second most abundant *d*-block metal ion in human brain and an active component in enzymes and proteins,[1] Zn^{2+} plays an important role in life processes including gene expression and neurotransmission.[2]fThe extent of Zn^{2+} deficiency is also associated with physical growth retardation and neurological disorder such as cerebral ischemia and Alzheimer's disease (AD).[3] Therefore, there is an increasing demand for highly sensitive analytical methods for the detection of Zn^{2+}. The *in vivo* temporal and spatial detection of Zn^{2+} is challenging but essential to address Zn^{2+}-related issues. Tremendous efforts has been devoted to developing sensitive Zn^{2+}-monitoring approaches.[4] Amongst them, fluorescence spectroscopy is particularly useful owing to its high sensitivity, ease of use, and ability to facilitate real-time detection.[5] Previously published fluorescent Zn^{2+} probes based on organic dyes and inorganic nanoparticles are summarized in Table S1.

Lanthanide-doped upconversion nanoparticles (UCNPs), which are capable of converting near infrared (NIR) excitation light to short wavelength emissions, have emerged as a promising luminescent probe in potential applications in sensing and bioimaging owing to their intriguing characteristics, such as a large anti-Stokes shift of up to several hundred nanometers, non-autofluorescence from biosamples, high penetration depth and no photobleaching.[6] Alternatively, chromophores with specific recognition sites are widely used for highly selective sensing systems. Therefore, the integration of UCNPs and chromophores endows the hybrid system with the outstanding recognition properties of chromophores and remarkable imaging capacity from UCNPs, thus producing highly sensitive and selective sensing system based on fluorescence resonance energy transfer (FRET) process between them. Till now, a number of UCNPs-based FRET systems have been developed to detect various analytes, such as DNA,[7] O_2,[8] CN^-,[9] NH_4,[10] and Hg^{2+}.[11] To the best of our knowledge, UCNPs-based selective fluorescence probes for Zn^{2+} detection in real biological samples have yet been reported.

To address this need, we have developed multilayered UCNPs modified with polyacrylic acid and compound **1**, respectively, as probes (abbreviated as **1**-PAA-UCNPs

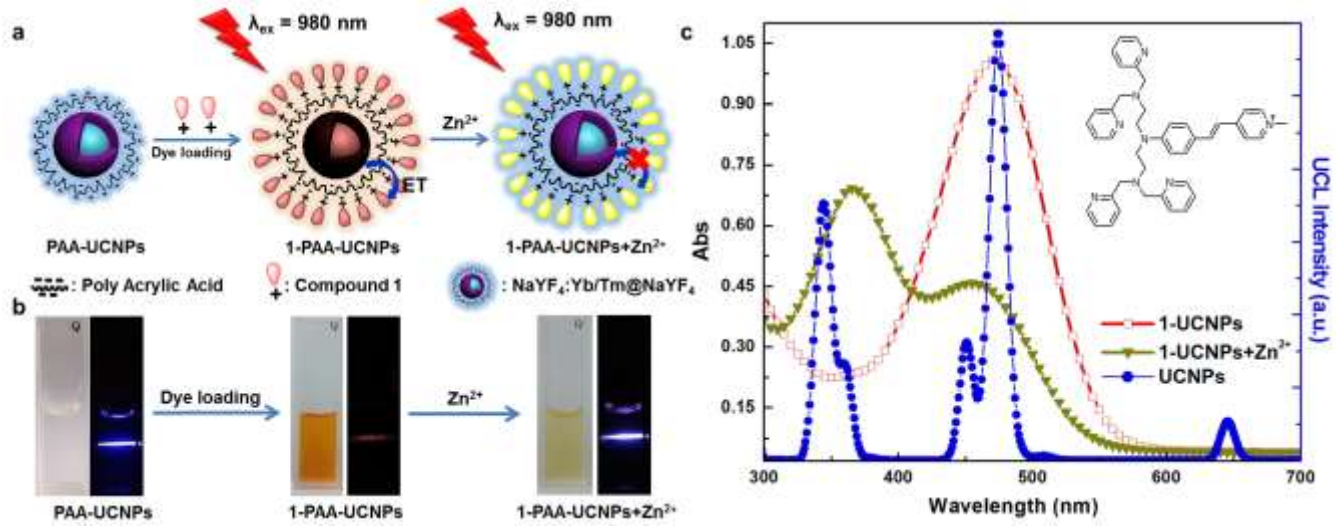

Figure 1. (a) Schematic illustration showing the synthesis of chromophore-assembled UCNPs and their response to Zn^{2+}. (b) Photographs showing the solution (left) and corresponding upconversion luminescence (right) of PAA-UCNPs (1 mg/mL), **1**-PAA-UCNPs (1 mg/mL) and **1**-PAA-UCNP with Zn^{2+} (120 μM), respectively. (c) UV-vis spectra of compound **1** measured in the absence (red line, 0.1 mM) and presence (dark yellow line, 120 μM) of Zn^{2+} and UCL spectrum of PAA-UCNPs (blue line). Inserted is the molecular structure of compound **1**.

shown in Figure 1) for sensitive and rapid monitoring of Zn^{2+} ions. A FRET process with $NaYF_4$:Yb/Tm@$NaYF_4$ (20/0.2 mol%) as the energy donor and Zn^{2+}-responsive compound **1** as the acceptor was constructed. Formation of a Zn-**1** complex inhibits the FRET, thus enabling the detection of Zn^{2+} in aqueous solution. Importantly, this hybrid nanoprobe is also applicable for upconversion luminescence (UCL) imaging of Zn^{2+}-rich amyloid brain tissues with AD. We further demonstrate its capability to detect endogenous Zn^{2+} in a living animal model of zebrafish.

■ RESULTS AND DISCUSSION

Design Principle of the UCL Nanosensor for Zn^{2+}. Our designed sensing system relies on a FRET process in **1**-PAA-UCNPs for detection of Zn^{2+} (Figure 1a). In this process, $NaYF_4$:Yb/Tm@$NaYF_4$ upconversion nanocrystals with blue UCL were used as energy donor. Alternatively, a Zn^{2+} responsive compound **1** assembled on the surface of upconversion nanocrystals was chosen as energy acceptor because of large overlapping between its absorption band with the UCL. In the absence of Zn^{2+}, the UCNPs give rise to blue emissions originating from the $^1G_4 \rightarrow {}^3H_6$ transition of Tm^{3+} under the excitation of a 980 nm laser. This UCL could be quenched by compound **1** with a strong absorbance band centered at 475 nm (Figure 1c), which is accompanied by the reduction in the $I_{475\ nm}/I_{654\ nm}$ ratio of UCL. In the presence of Zn^{2+}, the coordination of Zn^{2+} with the compound **1** could lead to a significant blue-shift of the absorbance of **1**-PAA-UCNPs from 475 to 360 nm due to the intramolecular charge transfer of compound **1** (Figure S1), thereby resulting in energy mismatch between the absorption of compound **1** and the blue emission of UCNPs. Therefore, the energy transfer (ET) from the UCNPs to compound **1** is suppressed, while the UCL signal located at 475 nm can be recovered. This variation in UCL intensity allows us to achieving quantitative monitoring of Zn^{2+}. On a separate note, the absorption band of compound **1** shows no overlap with the red emission ($^1G_4 \rightarrow {}^3F_4$ transition) of Tm^{3+} at 654 nm upon the addition of Zn^{2+}, which could be used as an inner reference to determine the Zn^{2+} concentration.

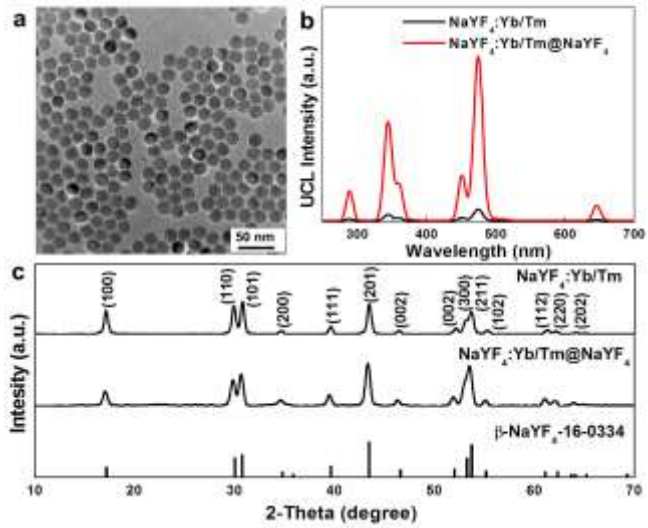

Figure 2. (a) TEM images of $NaYF_4$:Yb/Tm(20/0.2 mol%)@$NaYF_4$ core-shell nanocrystals. (b) The upconversion luminescence spectra of the $NaYF_4$:Yb/Tm (20/0.2% mol%) and $NaYF_4$:Yb/Tm(20/0.2% mol%)@$NaYF_4$ UCNPs under the 980 nm excitation. (c) X-ray powder diffraction pattern of the as-prepared $NaYF_4$:Yb/Tm core and $NaYF_4$:Yb/Tm@$NaYF_4$ core-shell nanoparticles, showing that all peaks can be well indexed in accordance with pure hexagonal $NaYF_4$ (JCPDS card No.15-0334).

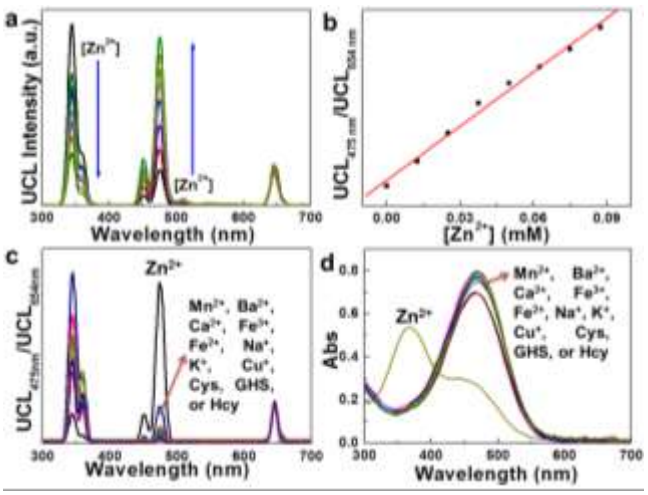

Figure 3. (a) Photoluminescence response of **1**-PAA-UCNPs solutions (1 mg/mL) as a function of Zn^{2+} concentration (0–0.09 mM) in an aqueous solution (normalized to 654 nm emission). (b Plot of luminescence intensity at $UCL_{475\,nm}/UCL_{654\,nm}$ against the Zn^{2+} concentration. (c) UCL spectra of **1**-PAA-UCNPs solutions (1 mg/mL) in the presence of different cations (0.1 mM each), amino acids and peptide (Cys, Hcy, GHS, 0.2 mM). (d) UV-Vis absorption spectra of **1**-PAA-UCNPs solutions (1 mg/mL) upon addition of different cations (0.1 mM), amino acids and GSH (0.2 mM).

Synthesis and Characterization of 1-PAA-UCNPs. In the present study, in order to obtain effective UCL, pure hexagonal-phase core-shell UCNPs with an average diameter of ~16 nm (Figure 2a, 2c, S2, and S3) were prepared according to the literature.[12] In a typical procedure, $NaYF_4$:Yb/Tm (20/0.2 mol%) nanocrystals were firstly synthesized as the core and subsequently coated by $NaYF_4$ shell through the epitaxial growth. The core-shell design can minimize surface quenching induced energy loss[13] and improve the UCL emission intensity by 10 times (Figure 2b). To integrate UCNPs and compound **1** together into one nanosystem, the oleic acid (OA) ligands on the surface of UCNPs were firstly replaced by negatively charged hydrophilic PAA.[14] It should be noted that the size and morphology of nanocrystals did not change during the ligand exchange process (Figure S4 and S5). Then the positively charged compound **1** was assembled onto the UCNPs surface through electrostatic attraction. With increasing concentrations of compound **1**, the UCL intensity of UCNPs remarkably decreased (Figure S6). The absorption spectroscopy result revealed that the amount of compound **1** on the surface of the UCNPs was 0.58×10^{-4} M, which was approximately 7.6 wt% of the **1**-PAA-UCNPs (Figure S7). To prove the stability of **1**-PAA-UCNPs in biological environments, the as-prepared nanoprobes were dispersed in different media, such as water, PBS (0.1 M, pH = 7.0), HEPES (1 M, pH = 7.0), DMEM medium (containing 10% FBS) or cell extracts, and kept for 24 hr prior to the measurement of UCL (Figure S8). It was found that the UCL signals remained essentially constant as compared to the non-incubated solution counterparts, clearly suggesting that the developed nanoprobe is feasible for applications in biological settings.

Zn^{2+}-Sensing Capabilities of 1-PAA-UCNPs. To examine the effect of Zn^{2+} concentration on the optical properties of **1**-PAA-UCNPs, we added different concentrations of Zn^{2+} into the aqueous solution containing as-prepared nanoprobes. As expected, upon addition of Zn^{2+} to the solution of **1**-PAA-UCNPs, a significant increase in the UCL intensity at 475 nm could be observed owing to the blue shift absorption of compound **1** (Figure 3a, 3b and S9). Significantly, we surprisingly found that the variation of color and UCL has fast response within 5 s. (Figure S10, movie in Supporting Information).

To further investigate the selectivity of **1**-PAA-UCNPs sensors, we tested a series of solution including various biological metal ions, amino acid including cysteine (Cys), homocysteine (Hcy), and glutathione (GHS). As shown in Figure 3c, only Zn^{2+} could induce obvious signal change of **1**-PAA-UCNPs. In contrast, other metal ions (e.g. Ca^{2+}, Fe^{3+}, Mn^{2+}, Ba^{2+}, Na^{+}, K^{+}) and amino acids did not result in any

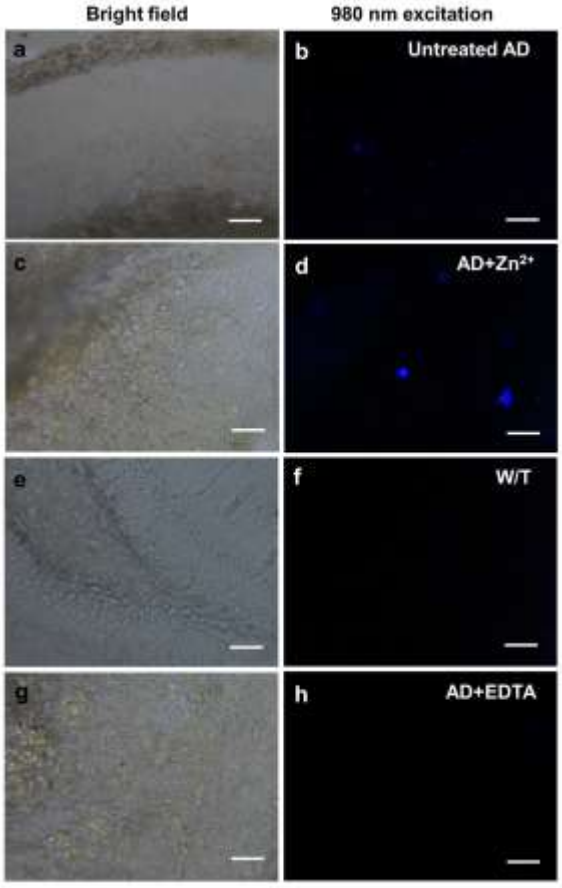

Figure 4. Bright-field and upconversion luminescence images of (a, b) AD brain tissue without treating, (c, d) AD brain tissue pre-incubation with 100 μM $ZnCl_2$ for 1 hr, (e, f) wild-type tissue (W/T), (g, h) AD brain tissue pre-incubation with 5 mM EDTA for 2 hr, then stained with **1**-PAA-UCNPs (500 μg/mL). The scale bars is 10 μm.

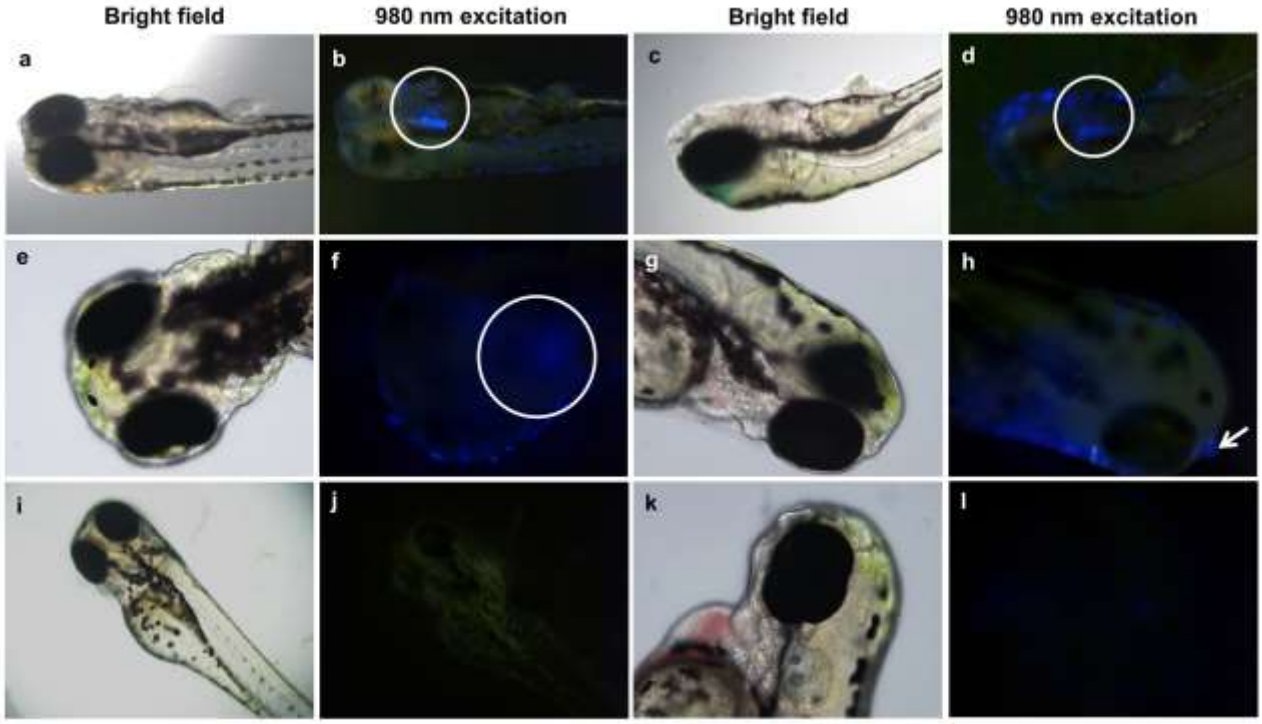

Figure 5. Bright-field (a, c, e, g) and upconversion luminescence images (b, d, f, h) of 3-day-old zebrafish incubated with 500 μg/mL **1**-PAA-UCNPs for 2 hr, bright-field (i, k) and upconversion luminescence images (j, l) of zebrafish incubated with EDTA 250 μM for 2 hr before 1-PAA-UCNPs (500 μg/mL) incubate for 2 hr, the total length is ~3 mm.

response of UCL signals. In addition, only the addition of Zn^{2+} led to drastic blue shift of the compound **1** absorption (Figure 3d), further suggesting the good selectivity of our sensor. Therefore, **1**-PAA-UCNPs could act as a highly selective UCL probe for Zn^{2+} *in vivo* without the interference from other metals

Sensing of Zn^{2+} in Living Cells. To demonstrate the potential use of **1**-PAA-UCNPs for bioimaging applications, the cytotoxicity of both PAA-UCNPs and **1**-PAA-UCNPs were evaluated on the basis of the reduction activity of methyl thiazolyl tetrazolium (MTT) assay. In our study, two kinds of cell lines (HeLa: cervical carcinoma and OSCC: oral squamous cell carcinoma) were selected. The cell viabilities of two cell line are both higher than 95% with the exposure of a dose of 600 μg/mL for 24 hr (Figure S11 and S12), suggesting that PAA-UCNPs and **1**-PAA-UCNPs have excellent biocompatibility. To investigate the capability of **1**-PAA-UCNPs for monitoring Zn^{2+} in cells, the cells were incubated with the nanoparticles (500 μg/mL) for 2 hr and analyzed under an optical fluorescence microscope equipped with a 980 nm laser. Blue UCL emitted by PAA-UCNPs without assembling of compound **1** can be clearly observed from the cells, indicating the cellular uptake of the PAA-coated nanoparticles (Figure S13a, b). On the other hand, only dim blue UCL can be observed from the cells treated with **1**-PAA-UCNPs (Figure S13c, d), while the blue UCL can be largely recovered by treatment of Zn^{2+} (0.25 mM) for 30 min (Figure S13 e, f). By monitoring variation of the UCL intensity from the cells in the presence or absence of Zn^{2+}, a semi-quantitative detection could be achieved (Figure S13 and S14). Taken together, these results confirm the feasibility of intracellular Zn^{2+} monitoring by **1**-PAA-UCNPs.

The Screening of β-Amyloid in Brain Tissue. AD is characterized by the presence of β-amyloid deposits in the brain, and oxidative stress has been implicated to play a crucial role in the pathogenesis.[15] Many recent studies have implicated metals to be crucial in the development or progression of AD.[16] Among these biometals, zinc is significant because of its ability to catalyze oxidative damage and modulate Alzheimer β-amyloid precursor protein processing.[17] To further validate the capability of our nanoprobes for monitoring Zn^{2+} ions in biological tissue, the triple transgenic knock-in mouse (APPsw/P301L tau/PSENM146) brain with AD was chosen as the model in our study owing to the high concentration of Zn^{2+} ions in the β-amyloid plaques.[18] We next incubated AD brain tissue with **1**-PAA-UCNPs and analyzed using a fluorescence microscope. As shown in Figure 4a and b, blue UCL spots can be observed from the brain tissue with AD treated by **1**-PAA-UCNPs. We further pre-treated brain slices with Zn^{2+}. After incubation with **1**-PAA-UCNPs, (Figure 4c and d), we surprisingly found that the pre-treatment led to much stronger UCL due to the concentrated Zn^{2+} in β-amyloid. To

verify that the UCL recovery originated from Zn^{2+}, wild-type brain tissue (W/T) from normal mouse was employed. As shown in Figure 4e and f, very weak UCL could be observed from imaging of the W/T tissue with a small amount of Zn^{2+}.[19] In another set of control experiment, EDTA was used to inhibit the coordination between compound **1** and Zn^{2+} owing to its strong chelation property. We pre-treated brain tissue with EDTA. As a result, almost no emission from brain tissue with **1**-PAA-UCNPs could be detected (Figure 4g, h), indicating good selectivity of our sensor. In addition, the comparison of UCL intensity from tissue images reveals that our probes enable the semi-qualitative detection of Zn^{2+} in brain tissue (Figure S15). Taken together, these results suggest that our designed nanoprobes can be promising probes for Zn^{2+} detection in biosamples.

***In Vivo* Zn^{2+} Detection in Zebrafish.** Encouraged by the results of the *in vitro* cell imaging and brain tissue studies, we further investigated the *in vivo* detection in living animal. In our experiment, zebrafish was chosen as model. The transparent zebrafish larva is an ideal animal model to monitor analytes using fluorescent sensors due to convenient detection of ions by fluorescence microscopy and permeability of ions and sensors in its body.[20] Therefore, zebrafish has been widely used to detect various ions such as Cu^{2+}, Ca^{2+} and Zn^{2+}.[21] As a proof of concept experiment, we incubated **1**-PAA-UCNPs with the living zebrafish and then traced the biodistribution of intact Zn^{2+} inside zebrafish by fluorescence microscopic imaging. As shown in Figure 5, the bright luminescence of **1**-PAA-UCNPs could be clearly observed around its ventricle (Figure 5b, d, f and h, encircled and arrow pointed). From the zoomed image of a part of the head in Figure 5h, it can be found that the bright luminescent dots were located at its eyes. We attributed it to the high concentration of Zn^{2+} in this position which might be the neuromasts of the anterior lateral-line system (ALL system) of zebrafish larva for the perception of the water flow.[22, 4b] As a control experiment, 3-day-old zebrafish were firstly exposed to EDTA (250 μM for 2 hr) before the treatment of **1**-PAA-UCNPs (Figure 5j, i). The imaging result shows that the obtained UCL signals in the fish significantly decreased. Furthermore, by quantitative analysis of UCL signals from the zebrafish before and after treatment with EDTA (Figure S16), it can also be found that the UCL intensity decreased significantly after EDTA treatment. All results suggest that the fluorescence is resulted from endogenous Zn^{2+} in zebrafish. Therefore, we can conclude that our **1**-PAA-UCNPs-based sensing system offers an exciting platform for *in vivo* Zn^{2+} detection.

■ CONCLUSIONS

In summary, we have developed a promising sensing platform using compound **1**-modified upconversion nanoprobes for rapid and sensitive detection of Zn^{2+} in aqueous solution. This detection nanosystem exhibited high sensitivity down to 0.78 μM and quick response within 5 seconds. Taking advantage of the good selectivity of compound **1** and the intriguing optical properties offered by UCNPs, we have also demonstrated our hybrid nanoprobes were also applicable for *in vitro* and *in vivo* Zn^{2+} detection in the amyloid plaque in AD brain and zebrafish, respectively. Our sensing system provides a new opportunity for disease diagnosis associated with Zn^{2+} in further clinical medicine.

■ EXPERIMENTAL SECTION

Materials. $Y(CH_3CO_2)_3{\cdot}xH_2O$ (99.9%), $Yb(CH_3CO_2)_3{\cdot}4H_2O$ (99.9%), $Tm(CH_3CO_2)_3{\cdot}xH_2O$ (99.9%), NaOH (98+%), NH_4F (98+%), 1-octadecene (90%), oleic acid (OA) (90 %) and HCl were purchased from Sigma-Aldrich and used as received without further purification.

Characterization. TEM measurements were carried out on a JEL-1400 transmission electron microscope (JEOL) operating at an acceleration voltage of 100 kV. UCL spectra were obtained with a DM150i monochromator equipped with a R928 photon counting photomultiplier tube (PMT), in conjunction with a 980 nm diode laser. UV-vis spectra were performed using a fluorimeter and UV/Vis instrument, SpectraMax M2, Molecular Devices. Cell imaging was performed on an Olympus BX51 microscope with a xenon lamp adapted to a 980 nm diode laser. The excitation laser power was adjusted to 2.5 W, and luminescence micrographs were recorded with a Nikon DS-Ri1 color imaging system. Image analysis was performed using NIS-Elements Advanced Research software (Nikon).

Synthesis of β-$NaYF_4$:Yb/Tm (20/0.2 mol%) Core Nanoparticles. In a typical experiment, a water solution (2 mL) containing $Y(CH_3CO_2)_3$ (0.32 mmol), $Yb(CH_3CO_2)_3$ (0.08 mmol) and $Tm(CH_3CO_2)_3$ (0.0008 mmol) was added to a 50 mL flask containing oleic acid (3 mL) and 1-octadecene (7 mL). The resulting mixture was heated to 150 °C for 1.5 hr to form lanthanide oleate complexes and remove water, and then cooled down to 50 °C. Subsequently, a methanol solution (6 mL) containing NH_4F (1.6 mmol) and NaOH (1 mmol) was added and stirred at 50 °C for 0.5 hr. The temperature of the reaction mixture was heated to 100 °C to remove the methanol. Upon removal of the methanol, the solution was heated to 290 °C for 1.5 h under an argon flow, at which time the mixture was cooled down to room temperature. The resulting nanoparticles were precipitated out by the addition of ethanol, collected by centrifugation, washed with ethanol and cyclohexane, and finally re-dispersed in cyclohexane.

Synthesis of $NaYF_4$:Yb/Tm@$NaYF_4$ Core-shell Nanoparticles. The core-shell nanoparticles were synthesized according to reported procedure.[23] To a 50 mL

flask containing oleic acid (3 mL) and 1-octadecene (7 mL) was added a solution of $Y(CH_3CO_2)_3$ (0.4 mmol) in water. The mixture was then heated to 150 °C for 1.5 hr with magnetic stirring and then cooled down to 50 °C. $NaYF_4$:Yb/Tm core nanoparticles in cyclohexane were added along with a 6 mL methanol solution of NH_4F (1.6 mmol) and NaOH (1 mmol). The resulting mixture was stirred at 50 °C for 30 min, at which time the reaction temperature was increased to 100 °C to remove the methanol. Then the solution was heated to 290 °C under an argon flow for 1 hr and cooled to room temperature. The resulting nanoparticles were precipitated out by the addition of ethanol, collected by centrifugation, washed with ethanol and cyclohexane, and re-dispersed in cyclohexane.

Preparation of Hydrophilic $NaYF_4$:Yb/Tm@$NaYF_4$ Core-Shell Nanoparticles. The preparation of the ligand free $NaYF_4$:Yb/Tm@$NaYF_4$ was performed as reported paper.[14a] Firstly, the OA ligands on the surface of $NaYF_4$:Yb/Tm@$NaYF_4$ were washed with hydrochloric acid and water-dispersible, ligand-free $NaYF_4$:Yb/Tm@$NaYF_4$ were obtained. Then ligand-free UCNPs were dispersed in 10 mg/mL PAA solution (adjusted to pH 7 with NaOH), followed by stirring for 12 hr, and PAA-UCNPs were obtained. Finally, the PAA-UCNPs were washed with distilled water by sonication and centrifugation.

Assembling compound 1 to PAA-UCNPs. 10 mM compound **1** in CH_2Cl_2 (0.2 mL) solution was added dropwise into a water solution containing PAA-UCNPs (1 mg/mL). The solution was then stirred overnight. Free compound **1** was removed by centrifugation. The precipitate was washed with water by centrifugation. The as-obtained hybrid materials (**1**-PAA-UCNPs) were re-dispersed by a brief sonication to form a homogeneous solution and stored at 4 °C.

Procedures for Ions Sensing. Stock solutions of the ions (2.5 mM) were prepared in H_2O. A stock solution of **1**-PAA-UCNPs (1 mg/mL) was prepared in water solution. The sensing of **1**-PAA-UCNPs to Zn^{2+} was performed by adding different amount of Zn^{2+} stock solution to 100 μL solution of **1**-PAA-UCNPs, respectively. Test samples for selectivity experiments were prepared by adding appropriate amounts of ions stock solution with a similar procedure, fluorescent spectra of the samples were recorded.

Movie. Real-time color change of **1**-PAA-UCNPs aqueous solution upon addition of Zn^{2+} aqueous solution (3 μL, 100 mM) was added, and the color was changed from orange to yellow within 5 seconds.

Cell Culture. The cell lines HeLa and OSCC cells were grown in DMEM medium supplemented with 10% (v/v) fetal bovine serum (FBS) and antibiotics (100 U/mL antibiotic /100 mg/mL antimycotic) in a humidified atmosphere at 37°C with 5% (v/v) CO_2.

Cytotoxicity of 1-PAA-UCNPs. To study the cytotoxicity, we dispensed 100 μL of cell suspension (~5000 cells/ well) in a 96-well plate. The cells were pre-incubated for 24 hr in high glucose media (DMEM) with 10 % fetal bovine serum (FBS) and 1% Anti-Anti with in a humidified incubator (37 °C, 5 %CO_2). Next, different concentrations of PAA-UCNPs, **1**-PAA-UCNPs (0, 100, 200, 300, 400, 500, and 600 μg/mL, diluted in DMEM) were then added to the wells. The cells were subsequently incubated for 12 or 24 hr at 37 °C under 5% CO_2. Then, MTT (20 μL, 5 mg/mL) was added to each well, and the plate was incubated for an additional 4 hr at 37 °C under 5% CO_2. After the addition of 100 μL DMSO, the assay plate was allowed to stand at room temperature for 2 hr. The optical density OD_{570} value (Abs) of each well, with background subtraction at 690 nm, was measured by means of a fluorimeter and UV/Vis instrument, SpectraMax M2, Molecular Devices. The following formula was used to calculate the inhibition of cell growth:

Cell viability(%)=(mean Abs value of treatment group/mean Abs value of control)×100%

Cell Imaging. HeLa and OSCC cell lines were maintained at 37 °C in 5% CO_2 in DMEM media respectively, both supplemented with 10% fetal bovine serum, 100 U/mL penicillin and 100 mg/mL streptomycin. The cells were plated at around 60-70% confluency 24 hr before imaging experiments in 35 mm culture dishes. Prior to imaging experiments, the cells were incubated with UCNPs (500 μg/mL), **1**-PAA-UCNPs (500 μg/mL) for 2 hr and the **1**-PAA-UCNPs treated cells incubated with Zn^{2+} (0.25 mM) solution for 30 min. Both cell lines were washed with cell culture media and subsequently imaged at ambient temperature.

Biological Sample Preparation. 15-20 months-old triple transgenic mice (APPsw/P301L tau/ PSENM146) were sacrificed for tissue harvesting. The mice were either perfused with 4 % (w/v) paraformaldehyde (PFA), or the brain tissue was rapidly frozen and stored at -80 °C immediately after extraction. Free-floating sections were prepared from the PFA-perfused brain using vibratome (Leica) and 40 □m slices were stored in anti-freeze solution at -20 °C until required. Separately, 10 μm sections of rapidly frozen brain were prepared using a cryostat and picked up on coated slides and stored in a -20 °C freezer.

Brain Tissue UCL *in Vivo* Imaging. Sections were mounted on slides, and then treated with 500 μg/mL **1**-PAA-UCNPs at room temperature. Separately, sections were pre-treated with 5 mM EDTA or 100 μM Zn^{2+} solutions for 1 hr before staining with **1**-PAA-UCNPs. Imaging was done with Nikon DS-Ri1 color imaging system.

Tracing Distribution of Zn^{2+} in Zebrafish. Zebrafish were kept at 28 °C and maintained at optimal breeding conditions. For mating, male and female zebrafish were maintained in one tank at 28°C on a 12 hr light/12 hr dark cycle, and then the spawning of eggs was triggered by giving light stimulation. Zebrafish were maintained in E3 embryo media. Zebrafish at 3 day were incubated with 500 μg/mL **1**-PAA-UCNPs for 2 hr at 28°C. Alternatively, 3 day zebrafish were exposed to 250 μM EDTA for 2 hr at 28 °C to remove intact Zn^{2+} in zebrafish firstly, then zebrafish were further incubated with **1**-PAA-UCNPs for 2 hr at 28 °C. The treated zebrafish were imaged by an Olympus BX51 microscope with a xenon lamp adapted to a 980 nm diode laser.

■ ASSOCIATED CONTENT

Supporting Information.

The synthetic details of compound **1**, reaction mechanism between compound **1** and Zn^{2+}, Table S1, Figure S1-S15. This material is available free of charge *via* the Internet at http://pubs.acs.org.

■ AUTHOR INFORMATION

Corresponding Author

Prof. Chang: chmcyt@nus.edu.sg

Author Contributions

‡These authors contributed equally. The manuscript was written through contributions of all authors. All authors have given approval to the final version of the manuscript.

■ ACKNOWLEDGMENT

The authors gratefully acknowledge the A*STAR Joint Council Office (JCO), Singapore (Grant 1231AFG028) for the financial support.

■ REFERENCES

(1) Nolan, E. M.; Lippard, S. J., *Acc. Chem. Res.* **2009**, *42*, 193.

(2) (a) Burdette, S. C.; Lippard, S. J., *Proc. Natl. Acad. Sci. U S A* **2003**, *100*, 3605. (b) Walkup, G. K.; Burdette, S. C.; Lippard, S. J.; Tsien, R. Y., *J. Am. Chem. Soc.* **2000**, *122*, 5644. (c) Kimura, E.; Aoki, S.; Kikuta, E.; Koike, T., *Proc. Natl. Acad. Sci. U S A* **2003**, *100*, 3731.

(3) Atwood, C. S.; Moir, R. D.; Huang, X.; Scarpa, R. C.; Bacarra, N. M. E.; Romano, D. M.; Hartshorn, M. A.; Tanzi, R. E.; Bush, A. I., *J. Biol. Chem.* **1998**, *273*, 12817.

(4) (a) Xu, Z.; Baek, K.-H.; Kim, H. N.; Cui, J.; Qian, X.; Spring, D. R.; Shin, I.; Yoon, J., *J. Am. Chem. Soc.* **2009**, *132*, 601. (b) Qian, F.; Zhang, C. L.; Zhang, Y. M.; He, W. J.; Gao, X.; Hu, P.; Guo, Z. J., *J. Am. Chem. Soc.* **2009**, *131*, 1460. (c) Datta, B. K.; Mukherjee, S.; Kar, C.; Ramesh, A.; Das, G., *Anal. Chem.* **2013**, *85*, 8369. (d) Wang, H.; Sun, C. L.; Yue, Y. H.; Yin, F. F.; Jiang, J. Q.; Wu, H. R.; Zhang, H. L., *Analyst* **2013**, *138*, 5576.

(5) (a) Wong, B. A.; Friedle, S.; Lippard, S. J., *J. Am. Chem. Soc.* **2009**, *131*, 7142. (b) Xu, Z.; Yoon, J.; Spring, D. R., *Chem. Soc. Rev.* **2010**, *39*, 1996. (c) Burdette, S. C.; Walkup, G. K.; Spingler, B.; Tsien, R. Y.; Lippard, S. J., *J. Am. Chem. Soc.* **2001**, *123*, 7831. (d) Guo, Z.; Kim, G.-H.; Shin, I.; Yoon, J., *Biomaterials* **2012**, *33*, 7818. (e) Meng, X. M.; Wang, S. X.; Li, Y. M.; Zhu, M. Z.; Guo, Q. X., *Chem. Commun.* **2012**, *48*, 4196. (f) Satapathy, R.; Wu, Y. H.; Lin, H. C., *Org. Lett.* **2012**, *14*, 2564.

(6) (a) Wang, Z. L.; Hao, J. H.; Chan, H. L. W., *J. Mater. Chem.* **2010**, *20*, 3178. (b) Chatterjee, D. K.; Yong, Z., *Nanomedicine-Uk* **2008**, *3*, 73. (c) Shen, J.; Sun, L. D.; Yan, C. H., *Dalton Trans.* **2008**, 5687. (d) Zhang, F.; Shi, Y. F.; Sun, X. H.; Zhao, D. Y.; Stucky, G. D., *Chem. Mater.* **2009**, *21*, 5237. (e) Chen, G.; Ohulchanskyy, T. Y.; Liu, S.; Law, W.-C.; Wu, F.; Swihart, M. T.; Ågren, H.; Prasad, P. N., *ACS Nano* **2012**, *6*, 2969. (f) Hou, Z. Y.; Li, C. X.; Ma, P. A.; Cheng, Z. Y.; Li, X. J.; Zhang, X.; Dai, Y. L.; Yang, D. M.; Lian, H. Z.; Lin, J., *Adv. Funct. Mater.* **2012**, *22*, 2713. (g) Wang, G. F.; Peng, Q.; Li, Y. D., *Acc. Chem. Res.* **2011**, *44*, 322. (h) He, M.; Huang, P.; Zhang, C. L.; Chen, F.; Wang, C.; Ma, J. B.; He, R.; Cui, D. X., *Chem. Commun.* **2011**,*47*, 9510. (i) Ju, Q.; Tu, D. T.; Liu, Y. S.; Li, R. F.; Zhu, H. M.; Chen, J. C.; Chen, Z.; Huang, M. D.; Chen, X. Y., *J. Am. Chem. Soc.* **2011**, *134*, 1323. (j) Wang, F.; Liu, X. G., *Chem. Soc. Rev.* **2009**, *38*, 976. (k) Zhou, J.; Liu, Z.; Li, F. Y., *Chem. Soc. Rev.* **2012**, *41*, 1323. (l) Zhang, F.; Haushalter, R. C.; Haushalter, R. W.; Shi, Y. F.; Zhang, Y. C.; Ding, K. L.; Zhao, D. Y.; Stucky, G. D., *Small* **2011**, *7*, 1972-1976. (m) Auzel, F., *Chem. Rev.* **2004**, *104*, 139. (n) Lehmann, O.; Kompe, K.; Haase, M., *J. Am. Chem. Soc.* **2004**, *126*, 14935. (o) Park, Y. I.; Kim, H. M.; Kim, J. H.; Moon, K. C.; Yoo, B.; Lee, K. T.; Lee, N.; Choi, Y.; Park, W.; Ling, D.; Na, K.; Moon, W. K.; Choi, S. H.; Park, H. S.; Yoon, S.-Y.; Suh, Y. D.; Lee, S. H.; Hyeon, T., *Adv. Mater.* **2012**, *24*, 5755. (p) Zhang, F.; Braun, G. B.; Shi, Y. F.; Zhang, Y. C.; Sun, X. H.; Reich, N. O.; Zhao, D. Y.; Stucky, G., *J. Am. Chem. Soc.* **2010**, *132*, 2850. (q) Sivakumar, S.; Boyer, J. C.; Bovero, E.; van Veggel, F. C. J. M., *J. Mater. Chem.* **2009**, *19*, 2392. (r) He, G. S.; Tan, L. S.; Zheng, Q.; Prasad, P. N., *Chem. Rev.* **2008**, *108*, 1245. (s) Dong, C. H.; van Veggel, F. C. J. M., *ACS Nano* **2009**, *3*, 123. (t) Liu, J.; Liu, Y.; Bu, W.; Bu, J.; Sun, Y.; Du, J.; Shi, J., *J. Am. Chem. Soc.* **2014**, *136*, 9701. (u) Wang, J.; Deng, R. R.; MacDonald, M. A.; Chen, B. L.; Yuan, J. K.; Wang, F.; Chi, D. Z.; Andy Hor, T. S.; Zhang, P.; Liu, G. K.; Han, Y.; Liu, X. G., *Nat. Mater.* **2014**, *13*, 157. (v) Xie, X. J.; Gao, N. Y.; Deng, R. R.; Sun, Q.; Xu, Q. H.; Liu, X. G., *J. Am. Chem. Soc.* **2013**, *135*, 12608. (w) Shen, J.; Chen, G. Y.; Vu, A.-M.; Fan, W.; Bilsel, O. S.; Chang, C.-C.; Han, G., *Adv. Opt. Mater.* **2013**, *1*, 644. (x) Min, Y. Z.; Li, J. M.; Liu, F.; Yeow, E. K. L.; Xing, B. G., *Angew. Chem.* **2014**, *126*, 1030. (y) Tian, G.; Gu, Z. J.; Zhou, L. J.; Yin, W. Y.; Liu, X. X.; Yan, L.; Jin, S.; Ren, W. L.; Xing, G. M.; Li, S. J.; Zhao, Y. L., *Adv. Mater.* **2012**, *24*, 1226. (z) Lai, J. P.; Zhang, Y. X.; Pasquale, N.; Lee, K.-B., *Angew. Chem., Int. Ed.* **2014**, *53*, 14419.

(7) (a). Zhang, P.; Rogelj, S.; Nguyen, K.; Wheeler, D., *J. Am. Chem. Soc.* **2006**, *128*, 12410. (b) Kumar, M.; Zhang, P., *Langmuir* **2009**, *25*, 6024.

(8) Achatz, D. E.; Meier, R. J.; Fischer, L. H.; Wolfbeis, O. S., *Angew. Chem., Int. Ed.* **2010**, *50*, 260.

(9) (a) Yao, L. M.; Zhou, J.; Liu, J. L.; Feng, W.; Li, F. Y., *Adv. Funct. Mater.* **2012**, *22*, 2667. (b) Liu, J. L.; Liu, Y.; Liu, Q.; Li, C. Y.; Sun, L. N.; Li, F. Y., *J. Am. Chem. Soc.* **2011**, *133*, 15276. Zhao, L. Z.; Peng, J. J.; Chen, M.; Liu, Y.; Yao, L. M.; Feng, W.; Li, F. Y., *ACS Appl. Mater. Inter.* **2014**, *6*, 11190.

(10) Mader, H. S.; Wolfbeis, O. S., *Anal. Chem.* **2010**, *82*, 5002.

(11) (a) Liu, Q.; Peng, J. J.; Sun, L. N.; Li, F. Y., *ACS Nano* **2011**, *5*, 8040. (b) Liu, Y.; Chen, M.; Cao, T. Y.; Sun, Y.; Li, C. Y.; Liu, Q.;

Yang, T. S.; Yao, L. M.; Feng, W.; Li, F. Y., *J. Am. Chem. Soc.* **2013**, *135*, 9869.

(12) Wang, F.; Deng, R. R.; Wang, J.; Wang, Q. X.; Han, Y.; Zhu, H. M.; Chen, X. Y.; Liu, X. G., *Nat. Mater.* **2011**, *10*, 968.

(13) (a) Boyer, J. C.; Manseau, M. P.; Murray, J. I.; van Veggel, F. C. J. M., *Langmuir* **2010**, *26*, 1157. (b) Zhao, L. Z.; Peng, J. J.; Huang, Q.; Li, C. Y.; Chen, M.; Sun, Y.; Lin, Q. N.; Zhu, L. Y.; Li, F. Y., *Adv. Funct. Mater.* **2013**, *24*, 363.

(14) (a) Bogdan, N.; Vetrone, F.; Ozin, G. A.; Capobianco, J. A., *Nano Lett.* **2011**, *11*, 835. (b) Cheng, L.; Yang, K.; Chen, Q.; Liu, Z., *ACS Nano* **2012**, *6*, 5605.

(15) Cirrito, J., Extracellular Amyloid-β Protein Dynamics in Alzheimer's Disease. In *Microdialysis in Drug Development*, Müller, M., Ed. Springer New York: 2013; Chapter 9, pp 163-178.

(16) (a) Adlard, P. A.; Bush, A. I., *J. Alzheimer's Dis.* **2006**, *10*, 145. (b) Crichton, R. R.; Dexter, D. T.; Ward, R. J., *Coord. Chem. Rev.* **2008**, *252*, 1189. (c) Barnham, K. J.; Bush, A. I., *Curr. Opin. Chem. Biol.* **2008**, *12*, 222.

(17) Bush, A. I.; Pettingell, W. H.; de Paradis, M.; Tanzi, R. E.; Wasco, W., *J. Biol. Chem.* **1994**, *269*, 26618.

(18) Reshmi R.; Ren M.; Maria D. Y.; Gemma C.; Mark A. S., George P.; Barry H.; Frank W., *Biochem. Biophys. Res. Commun.* **2009,** *382*, 91.

(19) Emily. L. Q.; Dylan W. D.; Christopher J. C., *Chem. Rev.* **2008**, *108*, 1517.

(20) Hutchinson, R. W.; Cox, A. G.; McLeod, C. W.; Marshall, P. S.; Harper, A.; Dawson, E. L.; Howlett, D. R., *Anal. Biochem.* **2005**, *346*, 225.

(21) Brustein, E.; Marandi, N.; Kovalchuk, Y.; Drapeau, P.; Konnerth, A., *Pflug. Arch. Eur. J. Phy.* **2003**, *446*, 766.

(22) Grant, K. A.; Raible, D. W.; Piotrowski, T., *Neuron* **2005**, *45*, 69.

(23) Wang, F.; Wang, J.; Liu, X. G., *Angew. Chem., Int. Ed.* **2010**, *49*, 7456.

■ SYNOPSIS TOC